Published in final edited form as:
J Phys Chem C Nanomater Interfaces. 2008 October 9; 112(40): 15729–15734. doi:10.1021/jp805215j.

An Electrochemical Approach to and the Physical Consequences of Preparing Nanostructures from Gold Nanorods with Smooth Ends

Matthew J. Banholzer, **Shuzhou Li**, **Jacob B. Ketter**, **Dorota I. Rozkiewicz**, **George C. Schatz**[†], and **Chad A. Mirkin**[*]
Chemistry Department and International Institute for Nanotechnology, Northwestern University, 2145, Sheridan Rd, Evanston, IL 60208-3113, USA

Abstract

We have developed a method to smooth the end sections of nanowires and nanograps generated via the On-Wire Lithography process and studied these rods with optical spectroscopies and theoretical modeling (Discrete Dipole Approximation). The first step of the smoothing process is a reductive one aimed at controlling the diffusion and migration of metal ions to the growing nanorod surface by adjusting the applied potential and concentration of the metal ions in the growth solution. A second oxidative smoothing step, based in part on the energetic differences between topologically rough and smooth surfaces, is used to further smooth the nanorod. The RMS roughness can be reduced over five fold to approximately 5 nm. The properties of these smoothed rods were investigated by empirical and theoretical methods, where it was found the smoothed rods have sharper plasmon resonances and decreased SERS intensity.

INTRODUCTION

Recently, our group developed an electrochemistry based technique termed On-Wire Lithography (OWL), [1] which allows one to control the chemical composition and morphology of a nanorod. OWL allows one to make both positive (disk) and negative (gap) features along the long axis of the nanorod, with control over feature size and segment length down to the sub-5 nm size regime. As a result, OWL is a very versatile technique for manipulating the properties of nanorods, and it has led to a rapid way of prototyping interesting nanostructured materials and devices. These include: Raman active dispersible labels,[2] molecular electronic devices,[1,3] chemically powered nanorotors,[4] and electrical traps capable of localizing nanoscopic amounts of material in a gap that can be characterized electrically and by surface enhanced Raman spectroscopy (SERS)[5]. The wires made via OWL, and in fact all template based electrochemical processes,[6,7] typically exhibit large surface roughness at the segment ends. This roughness, which can be as large as ~8% of the rod diameter (30 nm RMS roughness for a 350 nm diameter rod), has a significant consequence with respect to both the optical and electrical properties of the rods and devices based upon them.

The topography of metal structures in general is of significant importance in a variety of areas relevant to chemistry, physics and nanoscience, including electrochemical response,[8,9] monolayer assembly,[10–12] electrical contact quality,[13] light scattering,[14] surface-enhanced

[†]for theoretical work: schatz@chemistry.northwestern.edu
[*]for experimental work: chadnano@northwestern.edu

Supporting Information Available. Additional experimental procedures and additional images of smoothed nanostructures.

Raman scattering (SERS),[15–19] plasmonics,[14,20,21] and the directed assembly of objects.[22] While many methods to modify the topology of bulk or thin-film metal surfaces exist, methods for smoothing the topography of nanorod surfaces do not exist, especially the segment ends where many of the interesting properties of the nanorod are significantly influenced. The lack of this capability is surprising considering hundreds of papers are published each year on such structures. Electropolishing, mechanical polishing,[23] and bulk high pressure methods,[24] which work well for micro and macroscale objects,[25] cannot be used effectively to control surface roughness with nanostructured rods.

Since nanowire growth is dominated by diffusion processes, by studying the deposition/diffusion processes underlying nanorod growth, it is possible to identify and optimize conditions that lead to smoother interfaces. Indeed, we have identified electrochemical conditions for smoothing the end surfaces of nanorods *in-situ* in a two step procedure, using relatively simple and widely accessible growth solutions and pulse sequences. The first step is a reductive one aimed at controlling the diffusion and migration of metal ions to the growing nanorod surface by adjusting the applied potential and concentration of the metal ions in the growth solution. A second oxidative smoothing step, based in part on the energetic differences between topologically rough and smooth surfaces, is used to further smooth the nanorod. This process also leaves the surface in a chemical state that supports further electrodeposition and the adsorption of ligands, including Raman active dyes with the appropriate surface binding functionalities. The nanorods with smooth ends allow one to study the relationship between surface roughness and their optical (plasmonic) properties, and more importantly, one can now use this smoothing procedure to optimize a nanorod structure for a given application. Accordingly, we have systematically investigated these properties in the context of SERSs, UV-Vis-NIR spectroscopy, and discrete dipole approximation (DDA) computational methods and shown that one can produce structures with well-defined plasmonic features, tailorable SERS-response, and optical properties that can be nicely correlated with theoretical prediction.

RESULTS AND DISCUSSION

Prior to the smoothing steps, nanowires were fabricated via literature methods.[6,7] Anodic-aluminum oxide templates with an inner pore diameter of 350 nm were purchased from Whatmann. 125 nm of Ag was evaporated onto the back of each template to serve as a working electrode. The template was placed in an electrochemical cell with a platinum counter electrode and a Ag/AgCl- reference. Ag was electrodeposited (−800 mV, 2C) in the template from a commercially available plating solution (Technic Inc. 1025 RTU). The cell was subsequently rinsed and refilled with Ni- (Technic, Inc.; Nickel Sulfamate RTU) or Au- (Technic, Inc.; Orotemp 24 RTU) plating solutions, which were used to grow Ni or Au portions of the nanowires (−800 and −900 mV, respectively). Subsequent smoothing steps are described below. Upon completion of the growth and/or smoothing process, the template was first placed in a solution of methanol, 30% H_2O_2 and 28% NH_4OH (ratio of 4:1:1) for ~20 min to remove the Ag backing, rinsed, and placed in 3M NaOH for 1 hour under ultrasonication to dissolve the AAO. Finally, the rods were washed 4 times with water.

To prepare the rods with smooth ends, we have adopted a multistep process designed to control the diffusion of metal ions to the growing rods. The first step of the smoothing process is a reductive one where a higher-concentration gold plating solution is employed and electrodeposition is carried out in pulses at higher potentials than normally used. In a typical experiment, an aqueous gold solution is prepared by dissolving $KAu(CN)_2$ in Orotemp 24 (200 mg $KAu(CN)_2$:7 mL Orotemp 24, 0.1 M). Nitrogen is bubbled through this solution, and ions are deposited onto the existing nanorods in the AAO template in 1.5 second pulses at −1200 mV. In each pulse about 30 mC of charge is passed, and after each

pulse the system is returned to open circuit. Since the cell has a 1 cm-radius opening for the template and the template itself has about 40% porosity, the total working electrode surface area is ~1.3 cm^2. The system is allowed to re-equilibrate for 2 seconds between pulses (about 0.785 nm is plated per mC of charge, variation in pore widths preclude accuracy to ± 10%). This can be repeated until the desired smoothness (down to ~15 nm) and/or length is achieved, but a minimum charge of approximately 200 mC (~160 nm) is usually required to achieve quoted RMS roughness values. It should be noted that this rapid deposition phenomenon is not limited specifically to gold and can be employed on even non-noble metal surfaces such as nickel, for example (See SOM Fig. S2). Indeed, for short lengths the topography of the surface matches the topography below it, so it is possible to partially smooth the “bottom” end of the gold nanowire by first rapidly growing a layer beneath the Au section that can be dissolved (e.g. a smooth nickel layer can be deposited beneath a gold nanorod section and subsequently dissolved).

As a result of this first step, the “as made” rod ends (RMS roughness = 27.7 ± 6.2 nm) become both flattened and smoothed (RMS roughness = 14.0 ± 1.6 nm) (Fig. 1A, B, D, E). All RMS roughness values were calculated by selecting the relevant areas of an AFM trace and applying the following equation:

$$R_{rms}=\sqrt{\frac{1}{n}\sum_{i=1}^{n}x_i^2}=\sqrt{\frac{x_1^2+x_2^2+\cdots+x_3^2}{n}}$$

where each *n* value corresponds to a single (x, y) point in the selected area and each *x* value corresponds to a z-value associated with each point. In particular, features that were non-normal to the surface were flattened. Indeed, bulbous features are very effectively removed in this step.

In the second, oxidative step, the nanorod remains in the concentrated plating solution, and a mild oxidation potential (−260 mV) is applied until the ratio of final to initial current is below 1% (typically 3 minutes, 30 mC charge passed). AFM data obtained on the ends of the nanorods (see SOM for procedure) confirm that after the second smoothing step, the nanorod ends decrease in roughness from 14.0 ± 1.6 nm (after the first step) to 5.3 ± 1.7 nm (Fig. 1., C, F). Thus, after the two step smoothing procedure, the rod ends are over 5 times smoother than they were initially. When this smoothing procedure is used in conjunction with OWL to prepare nanogaps, the electrode walls that define the gaps are also smoother than the electrode walls that define the nanogaps prepared by the conventional OWL process (SOM Fig. S1).

This multistep process leads to structures with significantly smoother ends for several reasons. First, the initial reductive step of the smoothing process is designed to avoid ion depletion through pulsing and to maintain high local ion concentrations near the ends of the rods. This leads to more homogenous and uniform metal deposition. This step minimizes the roughness of the ends at the start of nanorod growth and avoids increasing surface roughness as the rod grows. Note that the more traditional constant growth processes lead to structures with rough ends because one is constantly depleting the metal ion near the electrode surface, leading to variable rates of deposition.[26] Rod end areas with higher curvature typically exhibit preferential growth under these low metal ion concentration conditions, which leads to greater surface roughnesses.[27] Applying a sufficiently large, constant over-potential to drive more ions to the surface and discourage preferential deposition onto conical (rough) areas would appear to solve this problem, but such conditions result in additional undesirable electrochemical reactions that foul the nanorod surface (e.g. decomposition or reduction of additives in the supporting electrolyte). Therefore, our strategy overcomes this

problem by applying an over-potential large enough to accelerate greater numbers of ions towards the surface, but small enough to not cause side reactions (such as solvent breakdown) in a pulsed manner. In doing so, the solution near the surface is allowed to re-equilibrate with the bulk solution before continuing deposition.

The pulsed deposition leads to more homogeneous growth, but it does not significantly reduce rod end surface roughness. The second slow oxidation step relies on both thermodynamic and kinetic components to reduce end surface roughness. The thermodynamic component pertains to the size-dependent electrochemical behavior of polyhedral nanoparticles, which has been investigated by multiple groups previously.[28–30] In studying the electrochemical oxidation of small metal nanoparticles, researchers have concluded that the surface free energy makes a repulsive contribution to the electrochemical potential, making such structures easier to oxidize. This contribution varies inversely with the radii of a given set of nanostructures, and as a consequence oxidation is enhanced at regions of highest curvature (sharp features). Therefore, with the rods studied here, oxidation is facilitated at the rough surface features relative to smooth ones, leading to smoother rod ends. [27]

In addition to the above process, during oxidation the distribution of electron energies at the surface of the electrode is near E_0 for the Au/Au^+ redox couple. When the applied potential is close to E_0, equilibrium is established at the surface of the electrode and only slightly favors oxidation of the electrode material. Therefore, some gold atoms are oxidized and move into solution, while a smaller amount are reduced onto the metal surface. This becomes important when taken in conjunction with the second aspect of the oxidation: the statistical probability of an oxidized species encountering the electrode (nanorod) surface and undergoing reduction to bulk metal. Gold atoms in topographically low points (relative to the “average” height) on the nanorod surface that oxidize are far more likely to encounter the nanorod surface again before moving out into solution than those atoms escaping from topographically higher points. Consequently, higher points—those features further out in solution—are more likely to permanently lose gold atoms than lower points.

To demonstrate that the nanorods smoothed by this technique have properties that are complementary to “as made” nanorods, experimental and theoretical studies were conducted to investigate their light scattering properties using UV-Vis-NIR and Surface Enhance Raman Scattering (SERS) spectroscopy. The theory study is based on the discrete dipole approximation (DDA) method.[31] This method for solving the electrodynamics associated with a metal nanoparticle interacting with light (represented as a plane wave), has been extensively applied to extinction and SERS spectra, and reasonable agreement with experiment has often been found.[32,33] In this method, the nanoparticles are represented as a cubic array of polarizable elements whose polarizability is determined from the nanoparticle dielectric function using a lattice dispersion relation. Dipoles are induced as a result of interaction of the particle with an incident field, and with the fields arising from the other dipoles. The extinction cross-section is given by:

$$C_{ext} = \frac{4\pi k}{\left|\vec{E}^{inc}\right|^2} \sum_{j=1}^{N} Im\left[\vec{E}_j^{inc,*} \bullet \vec{P}_j\right],$$

where $\vec{E}^{inc}$ and $\vec{P}_j$ are the incident field and the electric dipole moment of the j^{th} dipole, respectively. The field outside the nanoparticle is determined from the superposition of the incident wave and the fields from the induced dipoles.

To study the Rayleigh light scattering properties of the nanorods, extinction UV-Vis-NIR spectra of 1.5 μm-long smoothed and unsmoothed nanorods in D_2O were collected, Fig. 2, and compared with results from the DDA calculations.[34] (Note that there is a detector change at 850 nm, which causes a sudden jump in the spectrum, and therefore makes it difficult to compare intensities for wavelengths below and above this wavelength.) Rods of this size tend to have relatively broad surface plasmon resonance bands (as compared with smaller diameter nanorods), because of radiative damping effects. However, it is apparent that the smoothed nanorods (blue spectrum) exhibit more defined surface plasmon resonances than the "as made" rods (red spectrum), with broad peaks at 880, 1000 and 1280 nm, in addition to narrow peaks at 1400, 1570 and 1682 nm. These more distinct (and more intense) resonances are of practical interest, as detection technologies that rely on the plasmon resonance wavelength shifts to detect an analyte are most effective for structures with narrow and well-defined resonances. [35]

To interpret the results in Fig. 2, we have calculated the extinction spectrum for a smooth rod that is 1.5 μm in length (black curve) using the DDA method. This calculation shows broad longitudinal multipolar resonances at 880, 1000 and 1280 nm that match the smooth rod results nicely (one would expect the multipolar resonances to be more sensitive to nanorod end smoothing than transverse modes), however the sharp resonances at longer wavelength (≥1400 nm) are missing, and there is a resonant structure in the 650–690 nm range in the DDA results that is not seen in the experiments. The sharp resonances at ≥1400 nm are especially puzzling as such long wavelength resonances would typically be associated with rods that have a higher aspect ratio than has been considered here.[32] One explanation, which is compatible with this observation, is that some of the rods in the experiments have formed end-to-end dimers (for both rough and smooth rods). To test this hypothesis, we have taken spectra of end-smoothed 3 μm rods (taken as being a model for a 1.5 μm end-to-end dimer) that have been made using the same technique. These structures (green spectrum, Fig. 2) show sharp resonances at 1400, 1570 and 1700, in reasonable correspondence with the spectrum for the 1.5 blue μm smoothed rods (blue spectrum, Fig. 2). Differences in the shapes of the peaks might be due to differences between the 1.5 μm dimer and 3.0 μm monomer structures. We see additional resonances for the 3 μm results in the 600–700 nm range which match what is observed in the DDA calculations (these peaks may also be present in the experimentally observed 1.5 μm rods, but variation in rod lengths and other experimental factors could have convoluted peak resolution). We also see that the 3 μm results do not show resonances in the 800–1300 nm range, which we have previously assigned to monomer features. We conclude that the experimental results involve a superposition of spectra for 1.5 μm monomers and dimers. While this has complicated the interpretation somewhat, the effect of smoothing the rods is clear, with the most important change being the more noticeable resonances in the 800–1300 range.

To provide additional theory studies of the effect of smoothing the rods, extinction spectra were calculated for a 400 nm-long rod with varying end RMS roughness of 0, 4, 16, and 24 nm. (Here the vertical and horizontal roughness scales are taken to be the same. Studies where the vertical and horizontal roughness were allowed to be different gave results that are closely connected). A 400 nm rod was used instead of a 1.5 μm one for computational convenience. To model the end roughness, a perfectly smooth rod was created first, and then small cubic blocks were deposited onto one end of the rod until the desired roughness was reached.[36] The average length of the rod was 400 nm, and only one end of the rod was roughened. The resulting extinction spectra, Fig. 3, showed a broad resonance at about 600 nm. As end roughness increases, this feature clearly decreases in prominence, going from a near-peak to a nearly indistinguishable feature in the extinction spectrum. This mimics the behavior of the measured results in Fig. 2.

Using single-particle measurements, surface-enhanced Raman scattering (SERS) was used to study the variation in electromagnetic fields with surface roughness. SERS is a widely studied phenomenon,[15–19] and it is has been shown from both experimental and theoretical studies that the intensity of the observed signal is proportional to $<|E|^4>$ where E is the enhancement in electric field at the metal surface.[33] The correlation of local field with roughness is less well understood, although it is often considered that SERS activity increases with increasing roughness by amounts that exceed the "trivial" effect of increased surface area. To confirm that smoothing affects the Raman scattering enhancement of the nanorod ends, the rods were functionalized with *p*-mercapto aniline (rods mixed in 1 mM ethanol *p*MA solution for 1 hr and rinsed 3 times with ethanol), and a scanning confocal Raman microscope (Witec Alpha S300, 633 nm He-Ne laser source) was used to measure total Raman intensity over a 2D map. Fig. 4 contains integrated Raman intensities of nanorods with both unsmoothed (Fig. 4A) and smoothed (Fig. 4B) ends. The data in this figure represent the sample with the median intensity of each sample set (as made or smooth rods). On average, the smoothed rods have 4 times less activity than the unsmoothed rods. It is interesting to note, however, that the maximum observed intensity from an unsmoothed rod was over 16 times the maximum observed intensity from a smoothed rod. This shows that the smoothing procedure not only is effective at reducing the average Raman intensity of an ensemble, but it is particularly effective at removing large roughness features that lead to large SERS intensity enhancement spikes.

To better understand this behavior, the local electric fields $<|E|^4>$ associated with a 400 nm nanorod with varying end roughness ranging from 0 to 32 nm (RMS) were calculated (Fig. 5). Also, contours of the local electromagnetic field ($<|E|^2>$from these calculations are presented in Fig. 6. As end roughness increases, Figures 5 and 6 show that the local EM field intensity increases by roughly a factor of two, while the area weighted intensity increases by a factor of 50. The latter is likely an overestimate of the enhancement due to roughness, as it assumes that coverage scales linearly with surface area. However what we see from the results in Fig. 5 is that the observed change in intensity in going from a smooth to a rough surface can easily be a factor of 4, and that both increased field and increased surface area contribute to the result. The strong sensitivity of SERS intensity to roughness also explains how intensity spikes can occur. While the SEM AFM traces show a seemingly smoother overall profile than is modeled in the theory calculations, the lack of single-nm resolution in the SEM and ~10 nm radius of curvature of the AFM probe make imaging these small feature difficult, Fig. 1.

CONCLUSION

In conclusion, we have developed a technique to smooth the end surfaces of nanowires via an *in situ* two-step electrochemical process. By applying high potential pulsed deposition followed by a slow oxidation, it is possible to smooth the surfaces of nanorods by over five fold. The optical properties of these nanorods are significantly affected by the rod morphology. Indeed, the Raman intensity can be tailored, while surface plasmon resonances are shown to become more intense and sharper for smoother rods. The ability to create nanowires with smooth ends, and also gap structures with much smoother interfaces and well defined gaps, will significantly increase the scope of utility for OWL-generated structures, especially in the fabrication of novel diagnostic labels[2,5,33] and molecular transport junctions.[3]

Supplementary Material

Refer to Web version on PubMed Central for supplementary material.

Acknowledgments

CAM and GCS acknowledge the National Science Foundation (NSF) for support of this research. CAM is also grateful for a NSSEFF Fellowship. GCS acknowledges grants DMR-0520513 and DMR-0705741. MJB acknowledges the ECS 2008 Summer Research Fellowship

References

1. Qin L, Park S, Huang L, Mirkin CA. Science. 2005; 309:113–115. [PubMed: 15994551]
2. Qin L, Banholzer MJ, Millstone JE, Mirkin CA. Nano Lett. 2007; 7:3849–3853. [PubMed: 18041858]
3. Chen X, Jeon YM, Jang JW, Qin L, Huo F, Wei W, Mirkin C. J Am Chem Soc. 2008; 130:8166–8168. [PubMed: 18528994]
4. Qin L, Banholzer MJ, Xu H, Huang L, Mirkin CA. J Am Chem Soc. 2007; 129:14870–14871. [PubMed: 17988136]
5. Zheng G, Qin L, Mirkin CA. Angew Chem Int Ed. 2008; 47:1938–1941.
6. Martin CR. Science. 1994; 266:1961–1966. [PubMed: 17836514]
7. Routkevitch D, Bigioni T, Moskovits M, Xu JM. J Phys Chem. 1996; 100:14037–14047.
8. Jodie L, Conyers J, White HS. Anal Chem. 2000; 72:4441–4446. [PubMed: 11008781]
9. Stevenson KJ, Hatchett DW, White HS. Langmuir. 1996; 12:494–499.
10. Guo LH, Facci JS, McLendon G, Mosher R. Langmuir. 1994; 10:4588–4593.
11. Leopold MC, Black JA, Bowden EF. Langmuir. 2002; 18:978–980.
12. Losic D, Shapter JG, Gooding JJ. Langmuir. 2001; 17:3307–3316.
13. Weiss EA, Chiechi RC, Kaufman GK, Kriebel JK, Li Z, Duati M, Rampi MA, Whitesides GM. J Am Chem Soc. 2007; 129:4336–4349. [PubMed: 17358061]
14. Wang H, Fu K, Drezek RA, Halas NJ. Appl Phys B. 2006; 84:191–195.
15. Albrechet GM, Creighton JA. J Am Chem Soc. 1977; 99:5214–5219.
16. Fleischmann M, Hendra PJ, McQuillian AJ. Chem Phys Lett. 1974; 26:163–166.
17. Jeanmaire DL, Van Duyne RP. J Electroanal Chem. 1977; 84:1–20.
18. Tian ZQ, Ren B, Wu DY. J Phys Chem B. 2002; 106:9463–9483.
19. Zhang W, Cui X, Yeo BS, Schmid T, Hafner C, Zenobi R. Nano Lett. 2007; 7:1401–1405. [PubMed: 17447824]
20. Raether, H. Surface Plasmons on Smoother and Rough Surfaces and on Gratings. Springer; 1988.
21. Jung YS, Sun Z, Kim HK. Appl Phys Lett. 2005; 87:263116.
22. Chen M, Searson PC. Adv Mat. 2005; 17:2765–2768.
23. Saifislam M, Jung GY, Ha T, Stewart DR, Chen Y, Wang SY, Willians RS. Appl Phys A. 2005; 80:1385–1389.
24. Logeeswaran VJ, Chan ML, Bayam Y, Saifislam M, Horsley DA, Li X, Wu W, Wang SY, Williams RS. Appl Phys A. 2007; 87:187–192.
25. Van Gils S, Pen CL, Hubin A, Terryn H, Stijns E. J Electrochem Soc. 2007; 154:C175–C180.
26. Bard, AJ.; Faulkner, LR. Electrochemical Methods: Fundamentals and Applications. John Wiley & Sons; 2001.
27. Maus RG, McDonald EM, Wightman RM. Anal Chem. 1999; 71:4994–4950.
28. Makov G, Nitzan A, Brus LE. J Chem Phys. 1988; 88:5076–5085.
29. Plieth WJ. J Phys Chem. 1982; 86:3166–3170.
30. Zhang X, Hicks EM, Zhao J, Schatz GC, Van Duyne RP. Nano Lett. 2005; 5:1503–1507. [PubMed: 16178265]
31. Draine BT, Flatau PJ. J Opt Soc Am A. 1994; 11:1491–1499.
32. Millstone JE, Park S, Shuford KL, Qin L, Schatz GC, Mirkin CA. J Am Chem Soc. 2005; 127:5312–5313. [PubMed: 15826156]
33. Qin L, Zou S, Xue C, Atkinson A, Schatz GC, Mirkin CA. P Natl Acad Sci USA. 2006; 103:13300–13303.

34. Payne EK, Shuford KL, Park S, Schatz GC, Mirkin CA. J Phys Chem B. 2006; 110:2150–2154. [PubMed: 16471797]

35. Byun KM, Yoon SJ, Kim D, Kim SJ. J Opt Soc Am A. 2007; 24:522–529.

36. Barabási, AL.; Stanley, HE. Fractal Concepts in Surface Growth. Cambridge University Press; New York: 1995.

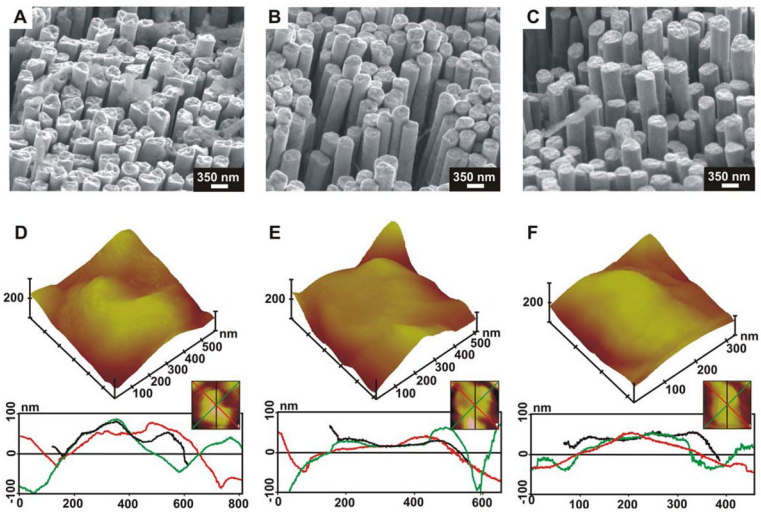

Figure 1.

SEM (top) and AFM images (bottom) of as-made (A, D), partially smoothed (B, E) and fully smoothed (C, F) nanorods. Under each AFM image are 2D profiles of "slices" taken to give a better sense of the topology of the surface; the color of each trace corresponds to the path indicated in the insert. Note the scale changes in the x axis in (F) are meant to emphasize the smoother features.

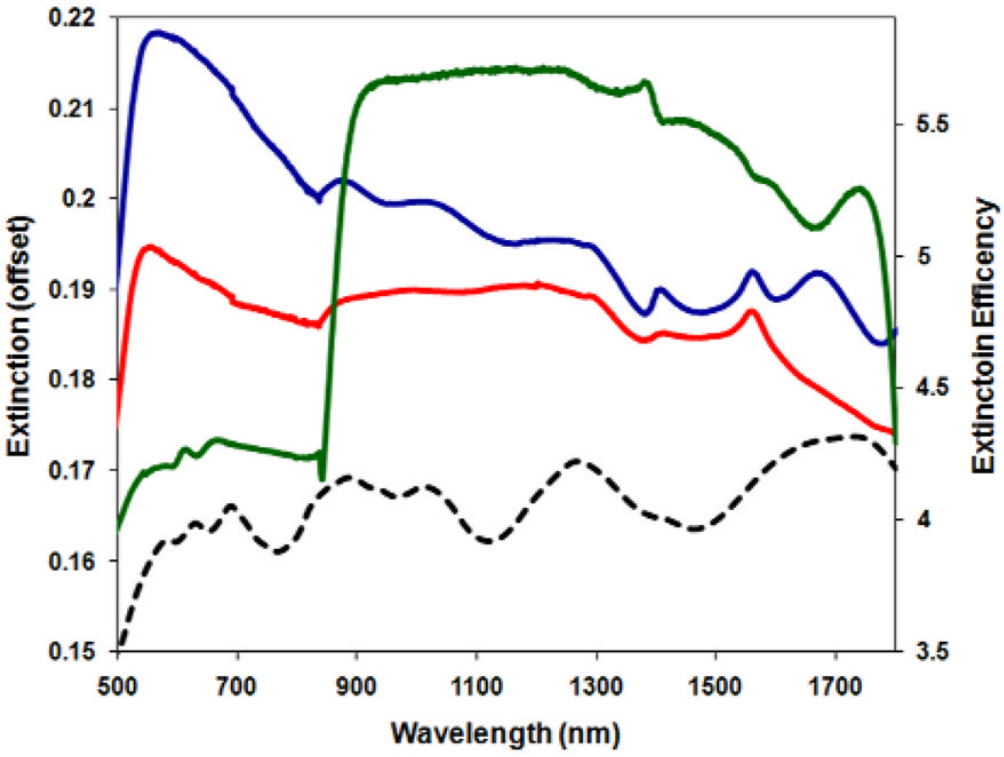

Figure 2.
Extinction spectra of smoothed and unsmoothed 350 nm-diameter nanorods. Blue line: 1.5 μm-long smoothed Au rods; red line: 1.5 μm-long as-made Au rods; green line: smoothed 3 μm Au rods. Dashed black line is the calculated extinction spectrum of a perfect 1.5 μm-long Au rod. Spectra artificially offset for clarity.

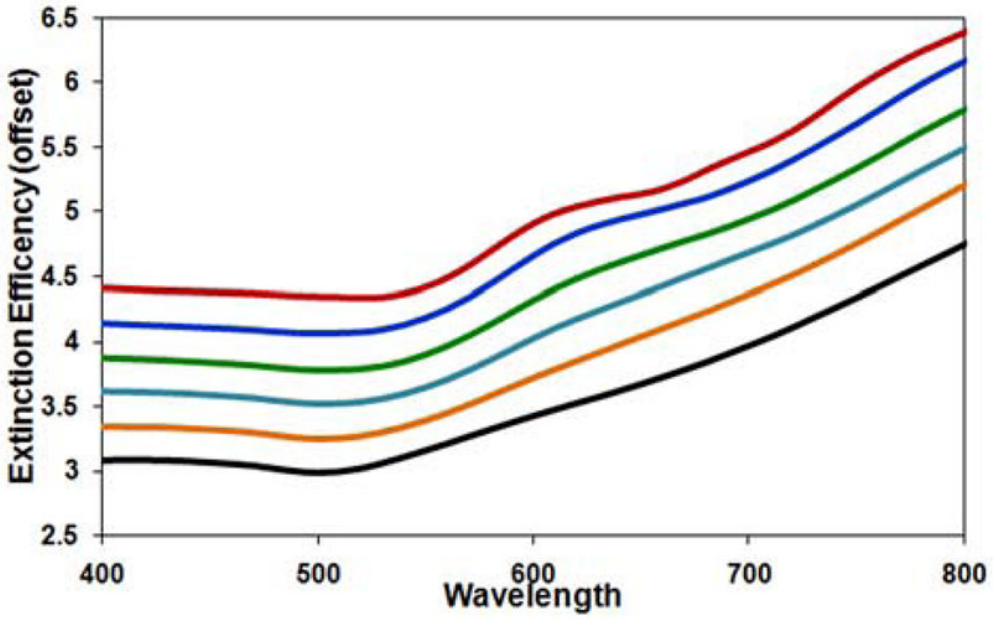

Figure 3.
Calculated extinction spectra for 350 nm-diameter, 400 nm-long Au rods with different RMS roughness. Red: 0 nm, Dark Blue: 4 nm, Green: 8 nm, Light Blue: 16 nm, Orange: 24 nm, Black: 36

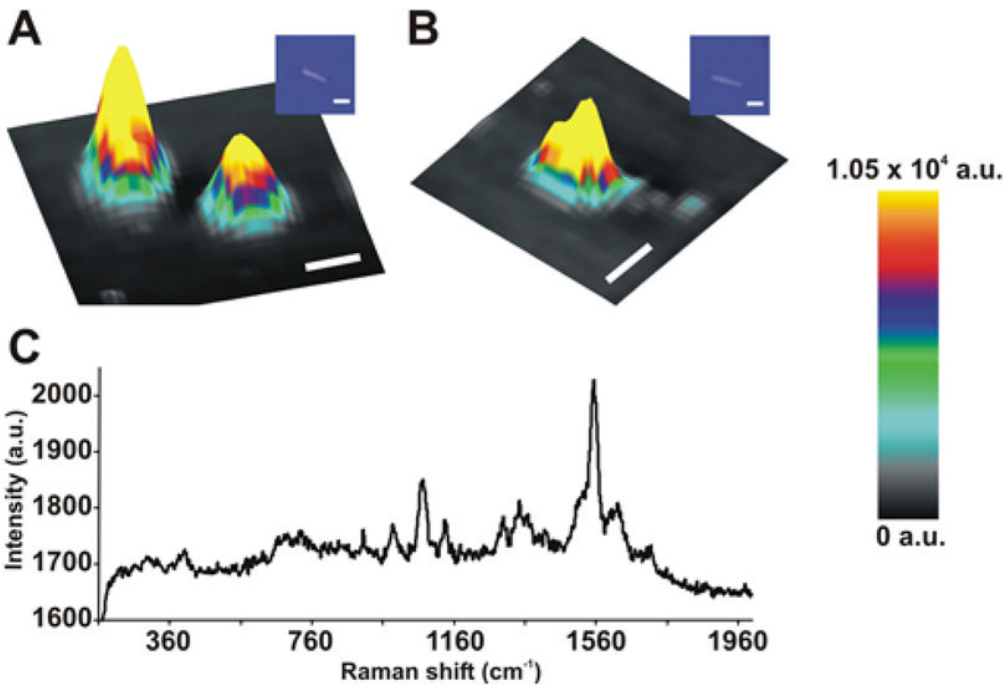

Figure 4.

Confocal Raman images of as-made (A) and smoothed (B) nanorods. In (B), the smoothed end is on the right side of the image (left end kept unsmoothed for comparison). Insert of optical microscopy image of the nanorods. Scale bar: 1 μm. (C) is a spectrum taken from an area of medium intensity in (A).

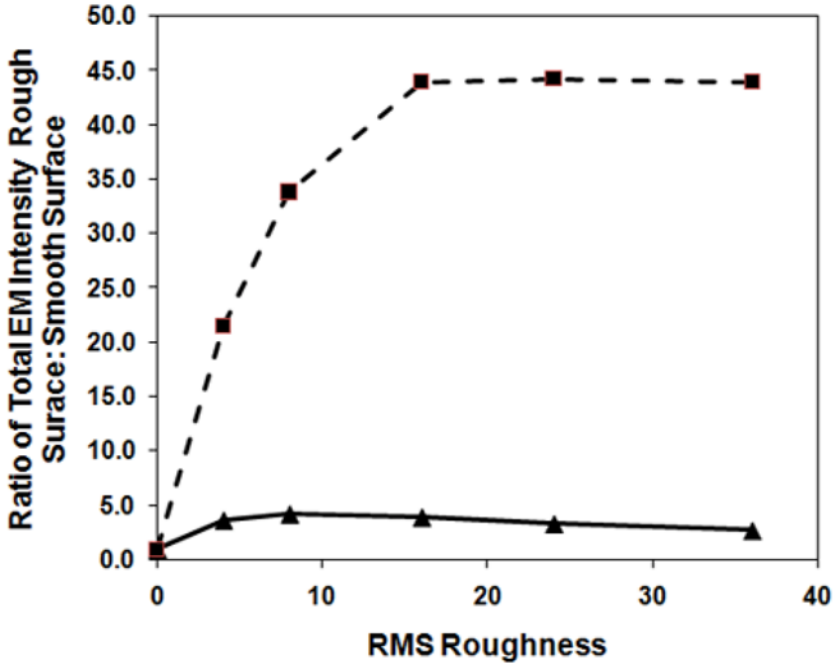

Figure 5.
Comparison of electromagnetic activity for nanorods as RMS roughness increases from 0 to 36 nm. The solid line is peak $<|E|^4>$. The dashed line is of $<|E|^4>$ *(Surface Area).

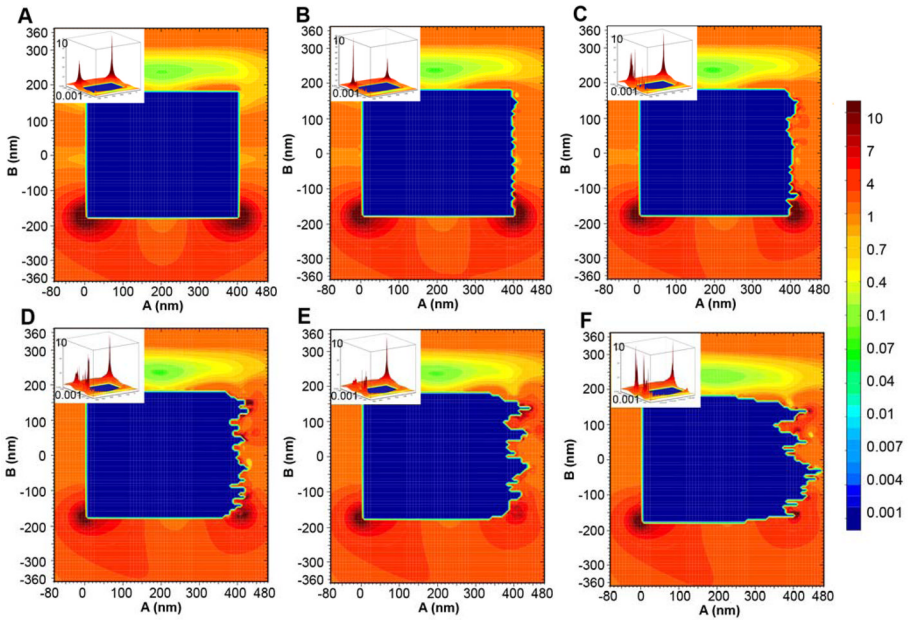

Figure 6.

Calculated $\langle|E|^2\rangle$ intensities of nanorods with RMS Roughness of 0 nm (A), 4 nm (B), 8 nm (C), 16 nm (D), 24 nm (E) and 36 nm (F). Color scale values are EM intensity relative to incident light (incident light value = 1). Inserts are 3D images of the same data with identical scales on the x and y axes. The z axis spans 0.001 to 10.